# Transient Analysis of a Semi-infinite Crack Subjected to Dynamic Concentrated Forces

**Chwan-Huei Tsai**[1]
Graduate Student.

**Chien-Ching Ma**[2]
Professor.

Department of Mechanical Engineering,
National Taiwan University,
Taipei, Taiwan, 10764,
Republic of China

*An exact transient closed-form solution for a semi-infinite crack subjected to a time-dependent concentrated force is obtained in this study. The total wave field is due to the effect of this point source and the scattering of the incident waves by the crack tip. An alternative methodology for constructing the reflected and diffracted field is proposed, which proves both powerful and efficient in solving complicated dynamic crack problems. An exponentially distributed loading at the crack surfaces in the Laplace transform domain is used as the fundamental problem. The waves reflected by the traction-free crack surface and diffracted from the crack tip can be constructed by superimposing this fundamental solution. The superposition is performed in the Laplace transform domain. Numerical results for the time history of stresses and stress intensity factors during the transient process are obtained and compared with the corresponding static values. It is shown that the field solution will approach the static value after the last diffracted wave has passed.*

## 1 Introduction

The interaction of a stress wave with a crack in an unbounded medium is a complicated problem. The incident wave will be reflected by the crack surface and diffracted from the crack tip. The analytical study of this problem is restricted to relatively simple cases. The investigation of transient elastodynamic crack problem was studied by de Hoop (1958) who analyzed the response of applying uniform normal pressure on the surfaces of a semi-infinite crack. Handelman and Rubenfeld (1969) investigated the reflection and diffraction of a horizontally polarized plane shear wave by a semi-infinite crack. Thau and Lu (1971) studied the diffraction of an incident longitudinal plane wave disturbed by a crack of finite length. They did not solve this problem completely. They used a solution to a semi-infinite crack to track the waves from one crack tip to the other, and stopped after one interaction. These problems were solved using the method of integral transforms together with the application of Wiener-Hopf technique (Noble, 1958) and Cagniard-de Hoop method (de Hoop, 1958) of Laplace inversion. Because there is no characteristic length involved, the integral transform can be applied directly and the standard Wiener-Hopf equation can be obtained. In a series of papers, Freund (1972a, 1972b, 1973, 1974a) developed important analytical methods for evaluating the transient field of a propagating crack. In Freund's papers, a fundamental solution is obtained and is used to develop by superposition the solution for the negation of the stress distribution on the prospective fracture plane. A generalization of this idea also led to solutions to problems in crack kinking under dynamic loading analyzed by Ma and Burgers (1987, 1988) and Ma (1988, 1990).

The problem of applied dynamic point loading on the crack surfaces was solved by Freund (1974b). Since this problem possesses a characteristic length, the distance from loading to crack tip, the Wiener-Hopf technique cannot be applied directly. Freund proposed a fundamental solution arising from a climbing edge dislocation with a constant speed. The transient response can be constructed by taking an integration over a climbing dislocation of different velocity. This methodology was also used by Brock (1982, 1984, 1985b, 1986, 1989), Brock et al. (1985a), Brock and Jolles (1987), and Ma and Hou (1991a, 1991b) to analyze other problems. Lee and Freund (1990) also applied this method to analyze fracture initiation of an edge crack due to impact loading.

In this paper, the two-dimensional problem of concentrated in-plane body force imposed suddenly near a semi-infinite crack is investigated. Brock (1985b) solved similar problems by superimposing Freund's solution (1974b) and obtained dynamic stress intensity factors only. But Brock's solution seems to be difficult in further application, since the multiple integrations are involved in his formulations. A similar but simpler problem was studied by Harris (1980), who solved the problem of diffraction by a stationary semi-infinite crack of a cylindrical longitudinal wave. In this study, we obtained not only the dynamic stress intensity factor but also the transient response of stresses. This problem can be treated as the superposition of two problems. The first problem is the disturbance by a concentrated force in the crack-free, unbounded medium. The second problem considers the crack surfaces subjected to the

[1]Currently at the Huafan Institute of Technology.
[2]To whom all correspondence should be addressed.

Contributed by the Applied Mechanics Division of THE AMERICAN SOCIETY OF MECHANICAL ENGINEERS for publication in the ASME JOURNAL OF APPLIED MECHANICS.

Discussion on this paper should be addressed to the Technical Editor, Prof. Leon M. Keer, The Technological Institute, Northwestern University, Evanston, IL 60208, and will be accepted until four months after final publication of the paper itself in the JOURNAL OF APPLIED MECHANICS.

Manuscript received by the ASME Applied Mechanics Division, Dec. 18, 1990; final revision, July 16, 1991. Associate Technical Editor: S. K. Datta.

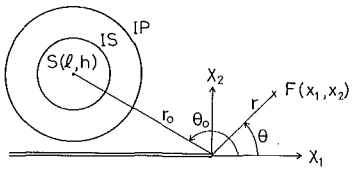


**Fig. 1 Configuration and coordinate systems of a semi-infinite crack in an infinite medium**

negatives of the tractions induced by the first problem. To solve this problem we propose an alternative fundamental solution of an applied exponentially distributed traction on crack surfaces in the Laplace transform domain. This methodology was first addressed by Tsai and Ma (1991) in solving the problem of an applied buried point loading in a half space. From the physical considerations, the reflected fields are generated in order to eliminate the stress induced by incident waves on the traction-free boundary. In a great number of dynamic problems, the incident waves can be represented by multiple Laplace transforms, so that the stress field in the Laplace transform domain (with respect to time) can be represented in a integral form for Laplace inversion (with respect to geometric coordinate) of which the kernel is usually an exponential function. Hence, if the responses to an applied exponentially distributed traction in Laplace transform domain can be obtained preliminarily, then the reflected and diffracted field can be constructed by the superposition method.

The analysis of the transient effect on the crack subjected to dynamic point loading is also investigated by numerical calculations using the available results. The characteristic time after which the transient effect can be neglected is investigated in detail. It is found in this study that the full-field solutions will approach the static value after the last diffracted wave has passed.

## 2 Required Fundamental Solutions

In this paper, an alternative fundamental solution is proposed and the superposition is made in the Laplace transform domain. The advantage is that the fundamental solution is easy to obtain and the solution is easy to construct. The wave motion generated by the diffraction of incident waves consists of the superposition of incident waves and the solutions of two fundamental problems, which are symmetric and antisymmetric with respect to the plane $x_2 = 0$.

Consider a stationary semi-infinite crack in an unbounded medium initially at rest. At time $t = 0$, an exponentially distributed traction is applied on the crack faces. The traction force can be divided into normal force (mode I) and tangential force (mode II). The geometry and coordinate system is shown in Fig. 1. Since it is a symmetrical problem with repect to the $x_1$-axis, it can be viewed as a half-plane problem with the material occupying the region $x_2 \geq 0$.

**2.1 Fundamental Solution of Mode I.** Consider the upper and lower crack faces to which are applied opposite normal traction with the following form:

$$\sigma_{22}(x_1,0,t) = \frac{1}{2\pi i}\int_{-\infty}^{\infty} \exp((p_1\eta_1 - p_2\eta_2)x_1 + p_1 t)\exp(i(p_2\eta_1 + p_1\eta_2)x_1 + p_2 t)dp_2 \quad \text{for} \quad -\infty < x_1 < 0. \tag{1}$$

Letting $p' = p_1 + ip_2$ and $\eta = \eta_1 + i\eta_2$, the special distribution of stress on the crack faces represented in Eq. (1) becomes

$$\sigma_{22}(x_1,0,t) = \frac{1}{2\pi i}\int_{p_1 - i\infty}^{p_1 + i\infty} e^{p'\eta x_1 + p't}dp' \text{ for } \quad -\infty < x_1 < 0, \tag{2}$$

with the other two boundary conditions

$$\sigma_{12}(x_1,0,t) = 0 \quad \text{for} \quad -\infty < x_1 < \infty, \tag{3}$$

$$u_2(x_1,0,t) \quad \text{for} \quad 0 < x_1 < \infty. \tag{4}$$

Applying of the Laplace transform over time $t$ by parameter $p$ to the boundary conditions (2)–(4) yields

$$\bar{\sigma}_{22}(x_1,0,p) = e^{p\eta x_1} \quad \text{for} \quad -\infty < x_1 < 0, \tag{5}$$

$$\bar{\sigma}_{12}(x_1,0,p) = 0 \quad \text{for} \quad -\infty < x_1 < \infty, \tag{6}$$

$$\bar{u}_2(x_1,0,p) = 0 \quad \text{for} \quad 0 < x_1 < \infty. \tag{7}$$

Equation (5) indicates the exponentially distributed loading in the Laplace transform domain. Applying the two-sided Laplace transform with respect to $x_1$ under the restriction of $\mathrm{Re}(\eta) > \mathrm{Re}(\lambda)$ and using the Wiener-Hopf technique, the final result of stress $\sigma_{22}$ in the Laplace transform domain is

$$\bar{\sigma}_{22}(x_1,x_2,p) = \frac{1}{2\pi i}\int [B_1(\eta,\lambda)e^{-p\alpha x_2 + p\lambda x_1} + B_2(\eta,\lambda)e^{-p\beta x_2 + p\lambda x_1}]d\lambda, \tag{8}$$

where

$$B_1(\eta,\lambda) = \frac{(b^2 - 2\lambda^2)^2(a+\eta)^{1/2}}{2(b^2 - a^2)(a+\lambda)^{1/2}(\eta - \lambda)(c - \lambda)(c + \eta)S_-(\lambda)S_+(\eta)},$$

$$B_2(\eta,\lambda) = \frac{2\beta\lambda^2(a-\lambda)^{1/2}(a+\eta)^{1/2}}{(b^2 - a^2)(\eta - \lambda)(c - \lambda)(c + \eta)S_-(\lambda)S_+(\eta)}, \tag{9}$$

$$\alpha = (a^2 - \lambda^2)^{1/2},\ \beta = (b^2 - \lambda^2)^{1/2},$$

$$S_\pm(\lambda) = \exp\left(-\frac{1}{\pi}\int_a^b \tan^{-1}\left[\frac{4\xi^2(\xi^2 - a^2)^{1/2}(b^2 - \xi^2)^{1/2}}{(b^2 - 2\xi^2)^2}\right]\frac{d\xi}{\xi \pm \lambda}\right). \tag{10}$$

$a = \sqrt{\rho/(\gamma + 2\mu)}$, $b = \sqrt{\rho/\mu}$, $a$, $b$ and $c$ are the slownesses of the longitudinal wave, shear wave and Rayleigh wave, $\mu$ and $\rho$ are the shear modulus and mass density, respectively, and $\gamma$ is the Lame elastic constant. To ensure $\mathrm{Re}(\alpha)$ (or $\beta$) $\geq 0$ everywhere in the $\lambda$-plane, branch cuts are introduced from $a$ (or $b$) to $\infty$, and from $-a$(or $-b$) to $-\infty$. The stress intensity factor of this problem in the Laplace transform domain can be expressed as

$$\bar{K}_I(p) = \lim_{x_1 \to 0^+} \sqrt{2\pi x_1}\,\bar{\sigma}_{22}(x_1,0,p) = -\sqrt{\frac{2}{p}}\,K_I^F(\eta), \tag{11}$$

where

$$K_I^F(\eta) = \frac{(a+\eta)^{1/2}}{(c+\eta)S_+(\eta)}. \tag{12}$$

**2.2 Fundamental Solution of Mode II.** Consider the same stationary semi-infinite crack as shown in Fig. 1. The tangential traction is applied on the upper and lower crack surfaces. The boundary conditions in the Laplace transform domain have the following forms:

$$\bar{\sigma}_{22}(x_1,0,p) = 0 \quad \text{for} \quad -\infty < x_1 < \infty, \tag{13}$$

$$\bar{\sigma}_{12}(x_1,0,p) = e^{p\eta x_1} \quad \text{for} \quad -\infty < x_1 < 0, \tag{14}$$

$$\bar{u}_1(x_1,0,p) = 0 \quad \text{for} \quad 0 < x_1 < \infty. \tag{15}$$

The stress field $\bar{\sigma}_{22}$ and stress intensity factor $\bar{K}_{II}$ expressed in the Laplace transform domain are

$$\bar{\sigma}_{22}(x_1,x_2,p) = \frac{1}{2\pi i}\int [B_3(\eta,\lambda)e^{-p\alpha x_2 + p\lambda x_1} + B_4(\eta,\lambda)e^{-p\beta x_2 + p\lambda x_1}]d\lambda, \tag{16}$$

$$\bar{K}_{II}(p) = -\sqrt{\frac{2}{p}}\, K^F_{II}(\eta), \tag{17}$$

where

$$B_3(\eta,\lambda) = \frac{-\lambda(b-\lambda)^{1/2}(b^2-2\lambda^2)(b+\eta)^{1/2}}{(b^2-a^2)(\eta-\lambda)(c-\lambda)(c+\eta)S_-(\lambda)S_+(\eta)}, B_4 = -B_3, \tag{18}$$

$$K^F_{II}(\eta) = \frac{(b+\eta)^{1/2}}{(c+\eta)S_+(\eta)}. \tag{19}$$

## 3 Green Functions of Semi-infinite Crack

In this paper, a semi-infinite crack subjected to a singular source of concentrated dynamic force is considered. The applied concentrated loading can be divided into the components which are perpendicular and parallel to the crack faces. The solution for an arbitrary applied loading direction can be constructed from the combination of the solutions for these two directions. Given that the problem considered in this study has two characteristic lengths, a direct attempt to solve this problem by transform and Wiener-Hopf techniques is apparently not applicable. The transient elastodynamic crack problem is solved by the superposition method in the Laplace transform domain. The exact expressions for the full-field solutions and mixed-mode stress intensity factors are obtained in this study. The solutions are composed of incident field, reflected field, and diffracted field denoted by superscripts of *I*, *R*, and *D*, respectively. The incident fields are the responses to loading applied to an unbounded medium. The reflected and diffracted waves are generated by applying opposite traction at the crack surface to eliminate the stress induced by incident wave.

**3.1 Vertical Concentrated Force.** We have a stationary semi-infinite crack extending over $-\infty < x_1 \le 0$. Initially, the body is stress-free and at rest. At time $t=0$, a vertical concentrated force is produced at position $(l,h)$. The two-dimensional geometry of the problem is shown in Fig. 1. The time dependence of the loading is represented by the Heaviside step function $H(t)$. As shown in Achenbach (1973), the incident fields at $x_2 = 0$ expressed in the Laplace transform domain are

$$\bar{\sigma}^I_{22} = \frac{1}{2\pi i}\int [A_{11}(\lambda)e^{-p\alpha h + p\lambda(x_1-l)} + A_{12}(\lambda)e^{-p\beta h + p\lambda(x_1-l)}]d\lambda, \tag{20}$$

$$\bar{\sigma}^I_{12} = \frac{1}{2\pi i}\int [A_{13}(\lambda)e^{-p\alpha h + p\lambda(x_1-l)} + A_{14}(\lambda)e^{-p\beta h + p\lambda(x_1-l)}]d\lambda, \tag{21}$$

where

$$A_{11}(\lambda) = \frac{b^2-2\lambda^2}{2b^2},\ A_{12}(\lambda) = \frac{\lambda^2}{b^2},$$
$$A_{13}(\lambda) = \frac{\alpha\lambda}{b^2},\ A_{14}(\lambda) = \frac{-\lambda(b^2-2\lambda^2)}{2b^2\beta}. \tag{22}$$

The applied tractions on the crack face, in order to eliminate the incident wave as indicated in (20) and (21), have the functional form $e^{p\lambda x_1}$. The fundamental solutions for normal traction $e^{p\eta x_1}$ and tangential traction $e^{p\eta x_1}$ applied at crack faces have been solved in Section 2. The reflected and diffracted fields can be obtained by superimposing the incident wave tractions that are equal and opposite to (20) and (21). The result of the normal stress is

$$\bar{\sigma}_{22}(x_1,x_2,p) = \frac{1}{4\pi^2}\int_{\Gamma^\eta}\int_{\Gamma^\lambda} [(A_{11}(\eta)B_1(\eta,\lambda) + A_{13}(\eta)B_3(\eta,\lambda))e^{-p(\alpha^* h + \eta l)}e^{-p(\alpha x_2 - \lambda x_1)}d\lambda + (A_{11}(\eta)B_2(\eta,\lambda) + A_{13}(\eta)B_4(\eta,\lambda))e^{-p(\alpha^* h + \eta l)}e^{-p(\beta x_2 - \lambda x_1)}d\lambda + (A_{12}(\eta)B_1(\eta,\lambda) + A_{14}(\eta)B_3(\eta,\lambda))e^{-p(\beta^* h + \eta l)}e^{-p(\alpha x_2 - \lambda x_1)}d\lambda + (A_{12}(\eta)B_2(\eta,\lambda) + A_{14}(\eta)B_4(\eta,\lambda))e^{-p(\beta^* h + \eta l)}e^{-p(\beta x_2 - \lambda x_1)}d\lambda]d\eta, \tag{23}$$

where $\alpha^* = (a^2-\eta^2)^{1/2}$, $\beta^* = (b^2-\eta^2)^{1/2}$. Equation (23) constitutes a double inversion integral where the paths $\Gamma^\lambda$ and $\Gamma^\eta$ refer to Laplace inversion contours in the $\lambda$-plane and the $\eta$-plane, respectively. Here we shall carry out the inverse transformation using an extension of the Cagniard-de Hoop technique. In the usual case this technique enables two successive inversions to be performed in one step. In this particular problem we use the technique proposed by Harris (1980) to perform the three successive inversions. Let us start by inverting the first term of (23). We introduce Cagniard contours in both the $\eta$ and $\lambda$-plane by setting

$$\tau = \eta l + \alpha^* h, \tag{24}$$

$$t = -\lambda x_1 + \alpha x_2. \tag{25}$$

Equations (24) and (25) can be solved for $\eta$ and $\lambda$ to yield

$$\eta^\pm(\tau) = \frac{\tau}{r_0}\cos\theta_0 \pm i\sqrt{\frac{\tau^2}{r_0^2} - a^2}\,\sin\theta_0, \tag{26}$$

$$\lambda^\pm(t) = -\frac{t}{r}\cos\theta \pm i\sqrt{\frac{t^2}{r^2} - a^2}\,\sin\theta, \tag{27}$$

where $(r_0, \theta_0)$ and $(r, \theta)$ are the polar coordinates of the source point and field point, respectively, and

$$r_0 = \sqrt{h^2+l^2},\ \cos\theta_0 = \frac{l}{r_0},\ \sin\theta_0 = \frac{h}{r_0}, \tag{28}$$

$$r = \sqrt{x_1^2+x_2^2},\ \cos\theta = \frac{x_1}{r},\ \sin\theta = \frac{x_2}{r}. \tag{29}$$

In the $\eta$-plane (or $\lambda$-plane), (26) (or (27)) describes a hyperbola which is denoted as the Cagniard contour. We shift the $\eta$ and $\lambda$-integrations onto Cagniard contours along which $\tau$ and $t$ are both real and positive. In this technique, the two Cagniard contours must be superimposed in order to determine how and when they overlap for different locations of source and field points. Depending on this, the reflected and diffracted waves can be constructed automatically. Because $B_i(\eta,\lambda)$ possesses a pole at $\eta = \lambda$, the contribution of the pole at $\eta = \lambda$ and $\lambda = \eta$ has to be taken into account in the change of integral paths from $\eta$ to $\tau$ and $\lambda$ to $t$. Consider the deformed integral contour shown in Fig. 2(*a*). The requirement of $\mathrm{Re}(\eta) > \mathrm{Re}(\lambda)$ dictates that the integral path $\Gamma^\eta$ is always located at the right-hand side of $\Gamma^\lambda$. Recall from (23) that a pole term arises, representing the reflected waves. A source point denoted by $S_2(\theta_0 = 150$ deg) and two field points denoted by $F_1(\theta = 45$ deg) and $F_2(\theta = 15$ deg) are chosen to explain the generation of a reflected wave. At the field point $F_1$, where the integral path changes from $\eta$ to $\tau$, the pole at $\eta = \lambda$ will be embraced. The contribution of this pole represents the reflected RPP wave generated from the crack-free surface. But no pole should be taken into account for the field point $F_2$, meaning that the reflected RPP wave will not pass through $F_2$. It is concluded that the reflected RPP waves will pass the region for $\theta > \theta_2$, where $\theta_2 = \cos^{-1}((x_1-l)/r_2)$, $r_2^2 = (x_1-l)^2 + (x_2+h)^2$. The con-

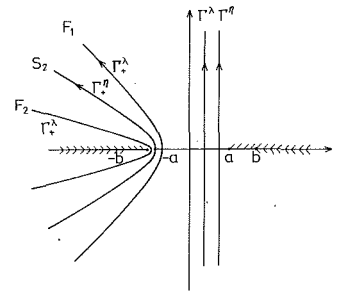


Fig. 2(*a*) Deformed integral contour for the first term of Eq. (23)

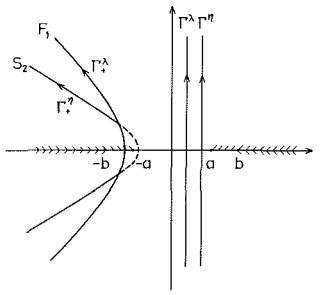


Fig. 2(*b*) Deformed integral contour for the second term of Eq. (23)

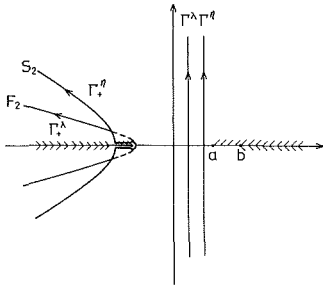


Fig. 2(*c*) Deformed integral contour for the third term of Eq. (23)

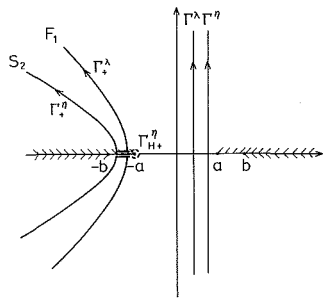


Fig. 2(*d*) Deformed integral contour for the fourth term of Eq. (23)

tribution of the pole in (23) can be obtained by the Cauchy theorem as follows:

$$\bar{\sigma}_{22}^{R}(x_1,x_2,p) = -\frac{1}{2\pi i}\int\left[\frac{(b^2-2\lambda^2)^3-4\alpha\beta\lambda^2(b^2-2\lambda^2)}{2b^2R}e^{-p\alpha(x_2+h)+p\lambda(x_1-l)} + \frac{4\alpha\beta\lambda^2(b^2-2\lambda^2)}{b^2R}e^{-p\beta x_2-p\alpha h+p\lambda(x_1-l)} + \frac{2\lambda^2(b^2-2\lambda^2)^2}{b^2R}e^{-p\alpha x_2-p\beta h+p\lambda(x_1-l)}\right]$$

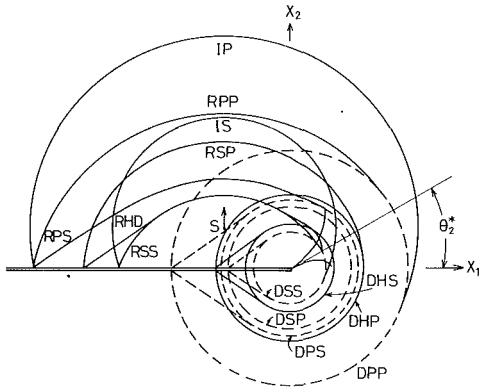


Fig. 3 Wave fronts of the incident, reflected, and diffracted waves with loading applied at $\theta_0 = 150$ deg

$$+\frac{4\alpha\beta\lambda^4-\lambda^2(b^2-2\lambda^2)^2}{b^2R}e^{-p\beta(x_2+h)+p\lambda(x_1-l)}\Bigg]d\lambda, \tag{30}$$

where $R(\lambda)$ is the Rayleigh wave function defined by

$$R(\lambda)=(b^2-2\lambda^2)^2+4\alpha\beta\lambda^2.$$

The superscript $R$ indicates that the reflected field is being considered. The first term of (30) represents the reflected RPP wave—the reflected primary wave from the incident primary wave. The other three terms in (30) are RPS, RSP, and RSS reflected waves, respectively. The reflected head wave RHD is contained in the last term of (30). A somewhat similar problem which has the same functional form as (30) arises from the reflection of a buried concentrated force from a traction-free half-space. For more details on the evaluation of (30), the reader is referred to Tsai and Ma (1991), which deals with the above problem. Some interesting phenomena of the reflected waves can be explained by the deformed integral contours shown in Figs. 2(*b*)–2(*d*). For the second term of (23), two Cagniard contours overlap for $\theta_2^*$ $(=\pi-\theta_0)<\theta<\cos^{-1}$ $(-a\cos\theta_0/b)$; see Fig. 2(*b*). This overlap would cause the RPS wave to distort in that region as shown in Fig. 3. Consider the third term of (23) and the deformed contours shown in Fig. 2(*c*). The overlap of these two Cagniard contours occurs in the region $0<\theta<\theta_2^*$. The integration path represented by the dash line will terminate at the intersection point of these two contours. This illustrates that the RSP wave is not complete in the region $0<\theta<\theta_2^*$ and only exists before the extended RSP wave from the crack tip arrives. Finally, consider the fourth term of (23) and the corresponding deformed contours shown in Fig. 2(*d*). The most important phenomenon is the distortion of the straight reflected head wave RHD at the right-hand side in the region, $\theta_2^*<\theta<\cos^{-1}(a/b)$. The threshold is determined from the intersection of $\Gamma_{H\pm}^{\eta}$ and $\Gamma_{\pm}^{\lambda}$, indicating that the straight wave front of the head wave will be deformed and terminated at the wave front of the DSS wave. The arrival time of these distorted wave fronts is presented in Eq. (A2) of the Appendix. By using the Cagniard-de Hoop method of the Laplace inversion, reflected fields in the time domain are represented in simple closed form and are shown in the Appendix.

Next we consider the diffracted waves generated from the crack tip. Here we shall carry out the inverse transformation for diffracted waves using an extension of the Cagniard-de Hoop technique. The deduction is explained in detail from the first term of (23). Recalling that $p$ is real and positive, we shift the $\eta$ and $\lambda$-integrations onto Cagniard contours. It can be written as

$$\bar{\sigma}_{22}^{\mathrm{DPP}}(x_1,x_2,p) = \frac{1}{2\pi^2}\int_{ar_0}^{\infty}\int_{ar}^{\infty} C_{1133}^{1}(\eta^{\pm}(\tau),\lambda(t))e^{-p(t+\tau)}dtd\tau, \quad (31)$$

where

$$C_{ijkl}^{m}(\eta^{\pm}(\tau),\lambda(t)) = \mathrm{Re}\left[(A_{mi}(\eta^{+}(\tau))B_j(\eta^{+}(\tau),\lambda(t))\right.$$
$$+ A_{mk}(\eta^{+}(\tau))B_l(\eta^{+}(\tau),\lambda(t)))\frac{\partial\eta^{+}(\tau)}{\partial\tau}\frac{\partial\lambda(t)}{\partial t}$$
$$-(A_{mi}(\eta^{-}(\tau))B_j(\eta^{-}(\tau),\lambda(t))$$
$$\left.+A_{mk}(\eta^{-}(\tau))B_l(\eta^{-}(\tau),\lambda(t)))\frac{\partial\eta^{-}(\tau)}{\partial\tau}\frac{\partial\lambda(t)}{\partial t}\right]. \quad (32)$$

From the Cagniard-de Hoop method, the inverse transform can be obtained by inspection and the DPP wave in the time domain can be expressed as

$$\sigma_{22}(x_1,x_2,t) = \frac{1}{2\pi^2}\int_{ar_0}^{t-ar} C_{1133}^{1}(\eta^{\pm}(\tau),\lambda(t'))d\tau, \quad (33)$$

where $t' = t-\tau$. The physical meaning of the DPP wave is the diffracted longitudinal wave induced by the incident IP wave and reflected RPP and RPS waves. The second term of (23) represents the DPS wave, the diffracted shear wave induced by the same waves that generate the DPP wave. There is a head wave DPH generated in the left-hand side of the crack tip by the additional branch cut at $\lambda = a$. The integral path $\Gamma^{\eta}$ of the third and fourth terms in (23) can be divided into two intervals $\Gamma^{\eta}_{H\pm}$ and $\Gamma^{\eta}_{\pm}$ as shown in Figs. 2(*c*) and 2(*d*). $\Gamma^{\eta}_{H\pm}$ represents the diffracted waves DHP, DHH, and DHS generated by RSP and RHD waves from the crack tip, while $\Gamma^{\eta}_{\pm}$ represents the diffracted waves DSP, DSH, and DSS induced by IS and RSS waves. Omitting the detailed deductions here, the stress caused by diffracted waves are found to be

$$2\pi^2\sigma_{22}^{D}(x_1,x_2,t) = \int_{ar_0}^{t-ar} C_{1133}^{1}(\eta_1^{\pm}(\tau),\lambda_1(t'))d\tau$$
$$+\int_{ar_0}^{t-t_H} C_{1234}^{1}(\eta_1^{\pm}(\tau),\lambda_2(t'))H(br-t')d\tau$$
$$+\int_{ar_0}^{t-br} C_{1234}^{1}(\eta_1^{\pm}(\tau),\lambda_3(t'))d\tau$$
$$+\int_{t_{H_0}}^{t-ar} C_{2143}^{1}(\eta_2^{\pm}(\tau),\lambda_1(t'))H(br_0-\tau)d\tau$$
$$+\int_{t_{H_0}}^{t-t_H} C_{2244}^{1}(\eta_2^{\pm}(\tau),\lambda_2(t'))H(br_0-\tau)H(br-t')d\tau$$
$$+\int_{t_{H_0}}^{t-br} C_{2244}^{1}(\eta_2^{\pm}(\tau),\lambda_3(t'))H(br_0-\tau)d\tau$$
$$+\int_{br_0}^{t-ar} C_{2143}^{1}(\eta_3^{\pm}(\tau),\lambda_1(t'))d\tau$$
$$+\int_{br_0}^{t-t_H} C_{2244}^{1}(\eta_3^{\pm}(\tau),\lambda_2(t'))H(br-t')d\tau$$
$$+\int_{br_0}^{t-br} C_{2244}^{1}(\eta_3^{\pm}(\tau),\lambda_3(t'))d\tau, \quad (34)$$

where

$$\eta_1^{\pm}(\tau) = \frac{\tau}{r_0}\cos\theta_0 \pm i\sqrt{\frac{\tau^2}{r_0^2}-a^2}\sin\theta_0,$$

$$\lambda_1(t') = -\frac{t'}{r}\cos\theta + i\sqrt{\frac{t'^2}{r^2}-a^2}\sin\theta,$$

$$\eta_2^{\pm}(\tau) = \frac{\tau}{r_0}\cos\theta_0 + \sqrt{b^2-\frac{\tau^2}{r_0^2}}\sin\theta_0,$$

$$\lambda_2(t') = -\frac{t'}{r}\cos\theta - \sqrt{b^2-\frac{t'^2}{r^2}}\sin\theta,$$

$$\eta_3^{\pm}(\tau) = \frac{\tau}{r_0}\cos\theta_0 \pm i\sqrt{\frac{\tau^2}{r_0^2}-b^2}\sin\theta_0,$$

$$\lambda_3(t') = -\frac{t'}{r}\cos\theta + i\sqrt{\frac{t'^2}{r^2}-b^2}\sin\theta,$$

$$t_{H_0} = r_0|\cos\theta_0| + r_0\sqrt{b^2-a^2}\sin\theta_0,$$

$$t_H = r|\cos\theta| + r\sqrt{b^2-a^2}\sin\theta. \quad (35)$$

The superscript D is used to indicate diffracted waves. Equation (34) contains nine terms which represent diffracted waves DPP, DPH, DPS, DHP, DHH, DHS, DSP, DSH, and DSS, respectively. The arrival time for each diffracted wave front is

$$T_{\mathrm{DPP}} = ar_0 + ar,\ T_{\mathrm{DPH}} = ar_0 + t_H,\ T_{\mathrm{DPS}} = ar_0 + br,$$
$$T_{\mathrm{DHP}} = t_{H_0} + ar,\ T_{\mathrm{DHH}} = t_{H_0} + t_H,\ T_{\mathrm{DHS}} = t_{H_0} + br,$$
$$T_{\mathrm{DSP}} = br_0 + ar,\ T_{\mathrm{DSH}} = br_0 + t_H,\ T_{\mathrm{DSS}} = br_0 + br. \quad (36)$$

The complete structures for the incident, reflected, and diffracted waves are represented in Fig. 3. Mixed-mode stress intensity factors in the Laplace transform domain can be represented as

$$\bar{K}_I(p) = \frac{\sqrt{2}}{2\pi i\sqrt{p}}\int [A_{11}(\eta)K_I^F(\eta)e^{-p\alpha^* h-p\eta l}$$
$$+A_{12}(\eta)K_I^F(\eta)e^{-p\beta^* h-p\eta l}]dd, \quad (37)$$

$$\bar{K}_{II}(p) = \frac{\sqrt{2}}{2\pi i\sqrt{p}}\int [A_{13}(\eta)K_{II}^F(\eta)e^{-p\alpha^* h-p\eta l}$$
$$+A_{14}(\eta)K_{II}^F(\eta)e^{-p\beta^* h-p\eta l}]dd. \quad (38)$$

Appling the Cagniard-de Hoop method for Laplace inversion, the stress intensity factors in the time domain can be obtained as follows:

$$\frac{\pi^{3/2}}{\sqrt{2}}K_I(t) = \int_{ar_0}^{t}\frac{1}{t-\tau}\mathrm{Im}\left[A_{11}(\eta_1^{+})K_I^F(\eta_1^{+})\frac{\partial\eta_1^{+}}{\partial\tau}\right]d\tau$$
$$+\int_{t_{H_0}}^{t}\frac{1}{\sqrt{t-\tau}}\mathrm{Im}\left[A_{12}(\eta_2^{+})K_I^F(\eta_2^{+})\frac{\partial\eta_2^{+}}{\partial\tau}\right]H(br_0-\tau)d\tau$$
$$+\int_{br_0}^{t}\frac{1}{\sqrt{t-\tau}}\mathrm{Im}\left[A_{12}(\eta_3^{+})K_I^F(\eta_3^{+})\frac{\partial\eta_3^{+}}{\partial\tau}\right]d\tau, \quad (39)$$

$$\frac{\pi^{3/2}}{\sqrt{2}}K_{II}(t) = \int_{ar_0}^{t}\frac{1}{\sqrt{t-\tau}}\mathrm{Im}\left[A_{13}(\eta_1^{+})K_{II}^F(\eta_1^{+})\frac{\partial\eta_1^{+}}{\partial\tau}\right]d\tau$$
$$+\int_{t_{H_0}}^{t}\frac{1}{\sqrt{t-\tau}}\mathrm{Im}\left[A_{14}(\eta_2^{+})K_{II}^F(\eta_2^{+})\frac{\partial\eta_2^{+}}{\partial\tau}\right]H(br_0-\tau)d\tau$$
$$+\int_{br_0}^{t}\frac{1}{\sqrt{t-\tau}}\mathrm{Im}\left[A_{14}(\eta_3^{+})K_{II}^F(\eta_3^{+})\frac{\partial\eta_3^{+}}{\partial\tau}\right]d\tau. \quad (40)$$

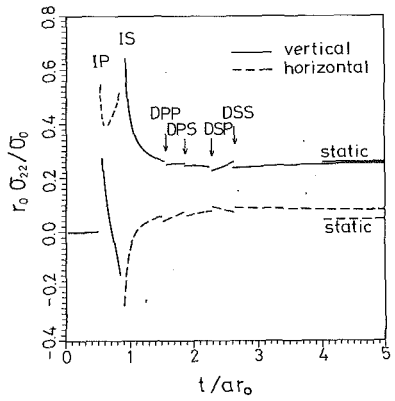


Fig. 4 Normal stress $\sigma_{22}$ at field point $F_1$ subjected to concentrated force applied at source point $S_1$

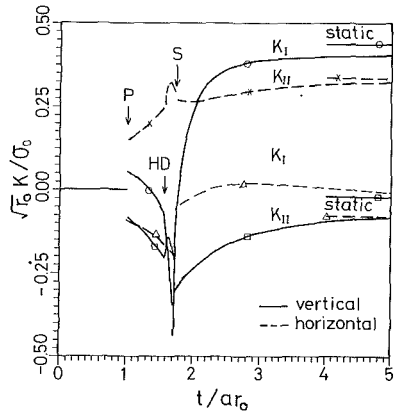


Fig. 6 Stress intensity factors $K_I$ and $K_{II}$ subjected to concentrated force applied at source point $S_2$

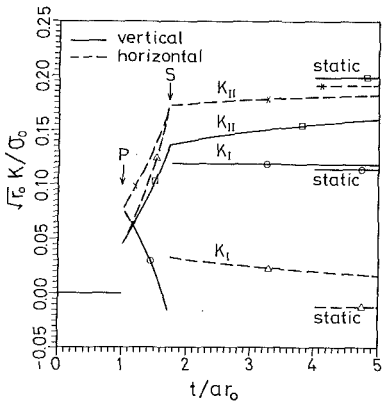


Fig. 5 Stress intensity factors $K_I$ and $K_{II}$ subjected to concentrated force applied at source point $S_1$

**3.2 Horizontal Concentrated Force.** Consider the same cracked body as shown in Fig. 1. Now the direction of the concentrated force is applied along the positive $x_1$ direction at the position $(l, h)$. Following the similar procedure of case (1) for the vertical direction, the diffracted waves and stress intensity factors can be represented in the same form as (34), (39), and (40) by replacing $C^1_{ijkl}$ by $C^2_{ijkl}$, and using the corresponding unknown functions $A_{2i}$

$$A_{21}(\eta)=\frac{\eta(b^2-2\eta^2)}{2b^2\alpha^*},\ A_{22}(\eta)=-\frac{\eta\beta^*}{b^2},$$
$$A_{23}(\eta)=\frac{\eta^2}{b^2},\ A_{24}(\eta)=\frac{(b^2-2\eta^2)}{2b^2}. \quad (41)$$

The procedure of finding incident and reflected waves can be obtained in the paper of Tsai and Ma (1991), and only the brief results are shown in the Appendix.

## 4 Numerical Results

The explicit analytical results for the stress $\sigma_{22}$ and the stress intensity factors have been given in the previous sections. For simplicity of the numerical calculation of the full-field solution, the source and field points are situated in such a manner that no reflected waves need be accounted for. A Poisson's ratio $\nu=0.25$ is used which gives ratios of wave speeds $b = \sqrt{3}a$ and $c = 1.88a$. The transient response of stress $\sigma_{22}$ for applied singular sources with Heaviside function dependence of concentrated force is shown in Fig. 4. The singular source is applied suddenly at the position $S_1(r_0, 45\text{ deg})$ and the transient stress $\sigma_{22}$ is evaluated at the field point $F(r_0/2, 45\text{ deg})$. There will be no reflected waves, only the incident waves (IP and IS) and diffracted waves (DPP, DPS, DSP, and DSS) will be generated. The time has been normalized by dividing by $ar_0$ and the arrival time for each wave front is indicated in the figures. The solid lines are valid for applying the singular source in the vertical $x_2$-direction while the dash lines are valid in the horizontal $x_1$-direction. The incident waves for the applied concentrated force have a singularity at their wave fronts while the diffracted waves have finite jumps at their wave fronts. The corresponding stress intensity factor is shown in Fig. 5. Next, a more complicated situation is considered in which the singular sources are applied at the position $S_2(r_0, 150\text{ deg})$. For this case, we evaluate only the time histories of dynamic stress intensity factors whose results are shown in Fig. 6.

In some classes of dynamic problems, the ability to find a static field may hinge on waiting for the wave fronts to pass and the transient effect to die away. The static solution obtained by Tada et al. (1973) for an applied static point force on a semi-infinite crack is used to construct the static solution and to compare with the transient result. It is found in this study that the transient full-field solutions for stress $\sigma_{22}$ will approach the corresponding static value after the last diffracted DSS wave has passed. The dynamic stress intensity factors will tend to the corresponding static values after the incident IS wave has arrived at the crack tip. The time needed for the transient field quantities to approach the static values depends on the direction of applied loading. If the loading is applied along the $x_2$-direction, then the time needed for $\sigma_{22}$ and $K_I$ to approach the static values will be less than that for $\sigma_{12}$and $K_{II}$.

In order to investigate the possibility of the crack surface interpenetration based on the transient solution obtained in this analysis, the vertical crack surface opening displacement is calculated for a vertical point loading in front of the crack tip ($\theta_0$ = 45 deg) and behind the crack tip ($\theta_0$ = 150 deg), respectively. In Fig. 7, the transient solution of opening displacement at different positions at the crack surface is evaluated for the vertical point loading in front of the crack tip. Where $u_2$ represents the difference of the displacement for the upper and lower crack surface, the contact of the crack surface will occur if $u_2$ is less than zero. It shows in this figure that the transient solution obtained in this study does predict contact of the crack surface, but the contact time is quite small. The general feature is that after the RSS wave has passed, the displacement at the upper and lower crack surface will move outward and the crack surface will be opened again. The contact time will be small if the material point is closed to the applied load. If the point loading is applied behind the crack tip, the transient displacement responses for five material points are plotted in Fig. 8. If the material points at the crack surface are directly below the applied loading (i.e., $r/r_0$= 1, 0.5), then

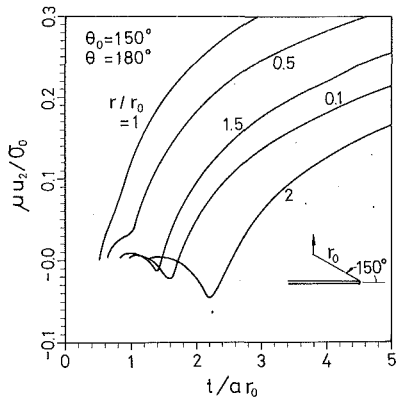


**Fig. 7 Vertical opening displacements of crack surfaces for applied concentrated load in front of the crack tip ($\theta_0$ = 45 deg)**

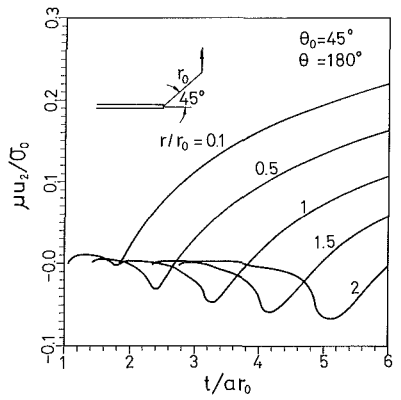


**Fig. 8 Vertical opening displacements of crack surfaces for applied concentrated load behind the crack tip ($\theta_0$ = 150 deg)**

there will be no contact for the whole time history. For the material points far from the applied load, the contact will occur but the contact time will be smaller than that for the loading applied in front of the crack tip. If the contact does occur at some material points, then the crack surface will be opened again after the RSS wave has passed.

## 5 Conclusions

The difficulty in determining the transient stress field in a cracked body subjected to dynamic loading is well known. It will become more complicated and difficult to solve if a characteristic length is involved in the analysis. The transient stress generated by the application of a concentrated force to a semi-infinite crack is obtained in an exact, closed form. A new fundamental solution is proposed for constructing the complicated reflected and diffracted waves generated by the crack. The fundamental problem is the application of exponentially distributed traction on the crack faces in the Laplace transform domain. Unlike the usual superposition method which is performed in the time domain, the transient solutions are determined by superposition of the fundamental solution in the Laplace transform domain. The extension of the Cagniard-de Hoop inverse method is used to investigate in detail the structure of the wave pattern.

In this paper we have obtained the transient response, at an arbitrary point in space and an arbitrary time, to waves reflected and diffracted in a semi-infinite crack which is struck by cylindrical incident waves generated by a concentrated force. The purpose was to investigate the characteristic time during which the transient effect is important. Numerical results for the analysis of transient effects are presented and compared to the corresponding static values. It is found that the dynamic transient solution will approach the static value after the last diffracted DSS wave has passed the field point.

## Acknowledgment

The authors gratefully acknowledge the financial support of this research by the National Science Council (Republic of China) under Grant NSC 79-0401-E002-36 and to the National Tawian University.

## References

Achenbach, J. D., 1973, *Wave Propagation in Elastic Solids*, Elsevier, New York.

Brock, L. M., 1982, "Shear and Normal Impact Loadings on One Face of a Narrow Slit," *International Journal of Solids and Structures*, Vol. 18, pp. 467-477.

Brock, L. M., 1984, "Stresses in a Surface Obstacle Undercut Due to Rapid Indentation," *Journal of Elasticity*, Vol. 14, pp. 415-424.

Brock, L. M., Jolles, M., and Schroedl, M., 1985a, "Dynamic Impact Over a Subsurface Crack: Applications to the Dynamic Tear Test," ASME JOURNAL OF APPLIED MECHANICS, Vol. 52, pp. 287-290.

Brock, L. M., 1985b, "The Dynamic 2D Analysis of a Concentrated Force Near a Semi-infinite Crack," *Quarterly of Applied Mathematics*, Vol. 43, pp. 201-210.

Brock, L. M., 1986, "Transient Dynamic Green's Functions for a Cracked Plane," *Quarterly of Applied Mathematics*, Vol. 44, pp. 265-275.

Brock, L. M., and Jolles, M., 1987, "Dislocation-Crack Edge Interaction in Dynamic Brittle Fracture and Crack Propagation," *International Journal of Solids and Structures*, Vol. 23, pp. 607-619.

Brock, L. M., 1989, "An Exact Transient Analysis of Dislocation Emission and Fracture," *Journal of the Mechanics and Physics of Solids*, Vol. 37, pp. 47-69.

de Hoop, A. T., 1958, "Representation Theorems for the Displacement in an Elastic Solid and Their Application to Elastodynamic Diffraction Theory," Doctoral Dissertation, Technische Hoegschool, Delft, The Netherlands.

Freund, L. B., 1972a, "Crack Propagation in an Elastic Solid Subjected to General Loading—I. Constant Rate of Extension," *Journal of the Mechanics and Physics of Solids*, Vol. 20, pp. 129-140.

Freund, L. B., 1972b, "Crack Propagation in an Elastic Solid Subjected to General Loading—II. Non-uniform Rate of Extension," *Journal of the Mechanics and Physics of Solids*, Vol. 20, pp. 141-152.

Freund, L. B., 1973, "Crack Propagation in an Elastic Solid Subjected to General Loading-III. Stress Wave Loading," *Journal of the Mechanics and Physics of Solids*, Vol. 21, pp. 47-61.

Freund, L. B., 1974a, "Crack Propagation in an Elastic Solid Subjected to General Loading—IV. Obliquely Incident Stress Pulse," *Journal of the Mechanics and Physics of Solids*, Vol. 22, pp. 137-146.

Freund, L. B., 1974b, "The Stress Intensity Factor Due to Normal Impact Loading of the Faces of a Crack," *International Journal of Engineering Science*, Vol. 12, pp. 179-189.

Handelman, G. H., and Rubenfeld, L. A., 1969, "Diffraction Of Horizontal Shear Waves by a Half Plane," ASME JOURNAL OF APPLIED MECHANICS, Vol. 36, pp. 873-874.

Harris, J. G., 1980, "Diffraction by a Crack of a Cylindrical Longitudinal Pulse," *Journal of Applied Mathematics and Physics*, Vol. 31, pp. 367-383.

Lee, Y. J., and Freund, L. B., 1990, "Fracture Initiation Due to Asymmetric Impact Loading of an Edge Cracked Plate," ASME JOURNAL OF APPLIED MECHANICS, Vol. 57, pp. 104-111.

Ma, C. C., and Burgers, P., 1987, "Dynamic Mode I and Mode II Crack Kinking Including Delay Time Effects," *International Journal of Solids and Structures*, Vol. 23, pp. 897-918.

Ma, C. C., and Burgers, P., 1988, "Initiation, Propagation, and Kinking of an Antiplane Crack," ASME JOURNAL OF APPLIED MECHANICS, Vol. 55, pp. 111-119.

Ma, C. C., 1988, "Initiation, Propagation, and Kinking of an In-plane Crack," ASME JOURNAL OF APPLIED MECHANICS, Vol. 55, pp. 587-595.

Ma, C. C., 1990, "Dynamic Mixed Mode I-II Crack Kinking under Oblique Stress Wave Loading in Brittle Solids," ASME JOURNAL OF APPLIED MECHANICS, Vol. 57, pp. 117-127.

Ma, C. C., and Hou, Y. C., 1991a, "Transient Analysis for Antiplane Crack Subjected to Dynamic Loadings," ASME JOURNAL OF APPLIED MECHANICS, Vol. 58, pp. 703-709.

Ma, C. C., and Hou, Y. C., 1991b, "Theoretical Analysis of the Transient Response for a Stationary Inplane Crack Subjected to Dynamic Impact Loading," *International Journal of Engineering Science*, in press.

Noble, B., 1958, *The Wiener-Hopf Technique*, Pergamon Press.

Thau, S. A., and Lu, T. H., 1971, "Transient Stress Intensity Factors for a Finite Crack in an Elastic Solid Caused by a Dilatational Wave," *International Journal of Solids and Structures*, Vol. 7, pp. 731-750.

Tada, H., Paris, P. C., and Irwin, G. R., 1973, *The Stress Analysis of Cracks Handbook*, Del Research Corporation, Hellertown, PA.

Tsai, C. H., and Ma, C. C., 1991, "Exact Transient Solutions of Buried Dynamic Point Forces and Displacement Jumps for an Elastic Half Space," *International Journal of Solids and Structures*, Vol. 28, pp. 955-974.

## APPENDIX

The Laplace transform of incident and reflected waves can be inverted immediately by the Cagniard-de Hoop scheme to give

$$\sigma_{22}(x_1,x_2,t)=\frac{1}{\pi}\sum_{j=1}^{6}\text{Im}\left[D_{ij}(\xi_j)\frac{\partial\xi_j}{\partial t}\right]H(t-T_j)+\frac{1}{\pi}\text{Im}\left[D_{i7}(\xi_7)\frac{\partial\xi_7}{\partial t}\right](H(t-T_7)-H(t-T_6)) \quad \text{(A1)}$$

where $i = 1,2$, representing the case of vertical and horizontal concentrated force, respectively. In which $j$ represents the IP, IS, RPP, RPS, RSP, RSS, and RHD waves, $j$ equals to 1 to 7, respectively. The reflected waves only exist in the region $\theta>\theta_2$, except the RSP wave. The distorted wave fronts of RPS, RSP, and RHD are shown in Fig. 3. The arrival times of the distorted wave front for the given regions are

$$T_{\text{RPS}}=\sqrt{\frac{b^2\sin^2\theta-a^2\sin^2\theta_0}{\cos^2\theta_0-\cos^2\theta}}\,(r_0\cos\theta-r\cos\theta_0) \quad \text{for } \theta_2^*<\theta<\cos^{-1}\left(-\frac{a}{b}\cos\theta_0\right),$$

$$T_{\text{RSP}}=\sqrt{\frac{b^2\sin^2\theta_0-a^2\sin^2\theta}{\cos^2\theta-\cos^2\theta_0}}\,(r_0\cos\theta-r\cos\theta_0) \text{ for } 0<\theta<\theta_2^*,$$

$$T_{\text{RHD}}=br-br_0\cos(\theta+\theta_0) \quad \text{for } \theta_2^*<\theta<\cos^{-1}\frac{a}{b}. \quad \text{(A2)}$$

The RSP wave in the distorted region ($0<\theta<\theta_2^*$) is valid in the time interval between arrival of the first RSP wave and $T_{\text{RSP}}$. The last term of (A1) represents the head wave which only exists in the region $b|\cos\theta_2|>a$. The unknown functions $\xi_j$, $D_{ij}$, and $T_j$ shown in (A1) can be found in Tsai and Ma (1991).